Human pluripotent stem cell-derived neural constructs for predicting neural toxicity

Michael P. Schwartz[a,1], Zhonggang Hou[b,1,2], Nicholas E. Propson[b], Jue Zhang[b], Collin J. Engstrom[c,d], Vitor Santos Costa[e], Peng Jiang[b], Bao Kim Nguyen[b], Jennifer M. Bolin[b], William Daly[a], Yu Wang[b,3], Ron Stewart[b], C. David Page[c,d], William L. Murphy[a,f], and James A. Thomson[b,g,h,4]

[a]Department of Biomedical Engineering, University of Wisconsin, Madison, WI 53706; [b]Regenerative Biology, Morgridge Institute for Research, Madison, WI 53715; [c]Department of Biostatistics and Medical Informatics, University of Wisconsin, Madison, WI 53792; [d]Department of Computer Sciences, University of Wisconsin, Madison, WI 53706; [e]Center for Research in Advanced Computing Systems, Institute for Systems and Computer Engineering, Technology and Science, and Department of Computer Science, Faculty of Sciences, University of Porto, Porto 4169-007, Portugal; [f]Department of Orthopedics and Rehabilitation, University of Wisconsin, Madison, WI 53705; [g]Department of Cell and Regenerative Biology, University of Wisconsin, Madison, WI 53705; and [h]Department of Molecular, Cellular, and Developmental Biology, University of California, Santa Barbara, CA 93106

Contributed by James A. Thomson, August 26, 2015 (sent for review April 3, 2015; reviewed by Fred H. Gage and Russell Thomas)

Human pluripotent stem cell-based in vitro models that reflect human physiology have the potential to reduce the number of drug failures in clinical trials and offer a cost-effective approach for assessing chemical safety. Here, human embryonic stem (ES) cell-derived neural progenitor cells, endothelial cells, mesenchymal stem cells, and microglia/macrophage precursors were combined on chemically defined polyethylene glycol hydrogels and cultured in serum-free medium to model cellular interactions within the developing brain. The precursors self-assembled into 3D neural constructs with diverse neuronal and glial populations, interconnected vascular networks, and ramified microglia. Replicate constructs were reproducible by RNA sequencing (RNA-Seq) and expressed neurogenesis, vasculature development, and microglia genes. Linear support vector machines were used to construct a predictive model from RNA-Seq data for 240 neural constructs treated with 34 toxic and 26 nontoxic chemicals. The predictive model was evaluated using two standard hold-out testing methods: a nearly unbiased leave-one-out cross-validation for the 60 training compounds and an unbiased blinded trial using a single hold-out set of 10 additional chemicals. The linear support vector produced an estimate for future data of 0.91 in the cross-validation experiment and correctly classified 9 of 10 chemicals in the blinded trial.

organoid | machine learning | tissue engineering | differentiation | toxicology

There is a pressing need for improved methods to assess the safety of drugs and other compounds (1–5). Success rates for drug approval are declining despite higher research and development spending (6), and clinical trials often fail due to toxicities that were not identified through animal testing (7). In addition, most of the chemicals in commerce have not been rigorously assessed for safety despite growing concerns over the potential impact of industrial and environmental exposures on human health (2–5). Animal models are costly, time consuming, and fail to recapitulate many aspects of human physiology, which has motivated agencies such as the National Institutes of Health (NIH) and the US Environmental Protection Agency (EPA) to initiate programs that emphasize human cellular approaches for assessing the safety of drugs (1) and environmental chemicals (2, 3). In vitro cellular models that accurately reflect human physiology have the potential to improve the prediction of drug toxicity early in the development pipeline (1) and would provide a cost-effective approach for testing other sources of chemical exposure, including food additives, cosmetics, pesticides, and industrial chemicals (2–5).

The human brain is particularly sensitive to toxic insults during development and early childhood (8), and there is growing concern that exposure to environmental chemicals may be linked to the rising incidence of neurodevelopmental disorders worldwide (4). Human brain development is mediated by highly coordinated cellular interactions between functionally distinct cell types that include neurons, glia, blood vessels, and microglia (9–15), each of which may be involved in neurotoxicity mechanisms (16–18). The cellular diversity of the developing brain complicates efforts to assess developmental neurotoxicity in vitro, because toxins might target numerous distinct cell types or cellular interactions and the underlying toxicity mechanisms are often unknown (3–5). Neurotoxicity has been evaluated using brain-derived cells in aggregate culture or coculture, neural stem cells, and other in vitro platforms, and these studies suggest that complex neurotoxic effects can be mimicked by incorporating cellular diversity into the model system (16, 18–20). However, many of these studies rely on animal cells that poorly reflect human physiology or primary human cells that are not scalable and introduce batch variability.

Although in vitro human cellular models have historically been hampered by inadequate access to cellular components of the human brain, human embryonic stem (ES) cells (21) and induced

Significance

Stem cell biology, tissue engineering, bioinformatics, and machine learning were combined to implement an in vitro human cellular model for developmental neurotoxicity screening. Human pluripotent stem cell-derived neural tissue constructs with vascular networks and microglia were produced with high sample uniformity by combining precursor cells on synthetic hydrogels using standard culture techniques. Machine learning was used to build a predictive model from changes in global gene expression for neural constructs exposed to 60 toxic and nontoxic training chemicals. The model correctly classified 9 of 10 additional chemicals in a blinded trial. This combined strategy demonstrates the value of human cell-based assays for predictive toxicology and should be useful for both drug and chemical safety assessment.

Author contributions: M.P.S., Z.H., N.E.P., J.Z., R.S., C.D.P., W.L.M., and J.A.T. designed research; M.P.S., Z.H., N.E.P., J.Z., C.J.E., V.S.C., B.K.N., J.M.B., W.D., and Y.W. performed research; M.P.S. and Z.H. contributed new reagents/analytic tools; M.P.S., Z.H., N.E.P., J.Z., C.J.E., V.S.C., P.J., R.S., and C.D.P. analyzed data; and M.P.S., Z.H., C.D.P., and J.A.T. wrote the paper.

Reviewers: F.H.G., The Salk Institute for Biological Studies; and R.T., Environmental Protection Agency.

Conflict of interest statement: W.L.M. is a founder and stockholder for Stem Pharm, Inc., and Tissue Regeneration Systems, Inc.

Freely available online through the PNAS open access option.

Data deposition: The data discussed in this publication have been deposited in NCBI's Gene Expression Omnibus (GEO) (Edgar et al., 2002) and are accessible through GEO Series accession number GSE63935 (www.ncbi.nlm.nih.gov/geo/query/acc.cgi?token=wfepekigrfqbfot&acc=GSE63935).

[1]M.P.S. and Z.H. contributed equally to this work.

[2]Present address: Department of Cell Biology, Harvard Medical School, Boston, MA 02115.

[3]Present address: State Key Laboratory of Stem Cell and Reproductive Biology, Institute of Zoology, Chinese Academy of Sciences, Beijing 100101, China.

[4]To whom correspondence should be addressed. Email: jthomson@morgridge.org.

This article contains supporting information online at www.pnas.org/lookup/suppl/doi:10.1073/pnas.1516645112/-/DCSupplemental.

pluripotent stem (iPS) cells (22, 23) now offer a scalable source for tissue-specific cell types. Here, reproducible 3D neural constructs that incorporated vascular and microglial components were fabricated for developmental neurotoxicity screening by culturing precursor cells derived from the H1 human ES cell line on synthetic hydrogels under defined conditions. Machine learning was used to build a predictive model from RNA sequencing (RNA-Seq) data for neural constructs exposed to a training set of 60 toxic and nontoxic chemicals and then to make predictions in a blinded trial using a set of 10 additional compounds.

Results

Cell types representing distinct components of the developing brain were derived from the H1 human ES cell line (*SI Appendix*, Fig. S1) (21), including neural progenitor cells (24), endothelial cells, mesenchymal stem cells (25), and microglia/macrophage precursors (*SI Appendix*, *SI Materials and Methods*). Vascular and microglial components were incorporated into the neural constructs to mimic the repertoire of cell types and cell–cell interactions of the developing human brain that might be susceptible to toxic exposure (16–18). The vascular component included both endothelial cells and mesenchymal stem cells, because mesenchymal support cells play an important role in the maintenance and long-term stability of vascular networks in vitro and in vivo (26). Neural tissue constructs were produced on peptide functionalized polyethylene glycol (PEG) hydrogels that were formed in 24-well Transwell inserts using "thiol-ene" photopolymerization (*SI Appendix*, Fig. S1) (27, 28). For these experiments, the time point when neural progenitor cells were seeded on the PEG hydrogels was defined as day 0. To mimic the in vivo recruitment of blood vessels and microglia after the initial formation of the neural tube (10–15), vascular cells and microglia/macrophage precursors were added at day 9 and day 13, respectively (*SI Appendix*, Fig. S1).

RNA-Seq was used to quantitatively assess sample reproducibility and to identify global gene expression patterns within the neural constructs. Replicate samples ($n = 4$) were characterized by Spearman's correlation coefficients (ρ) ≥ 0.97 at days 16 and 21 of growth on PEG hydrogels (Dataset S1) (29). Spearman's rank comparisons to RNA-Seq data for human samples from the Allen Brain Atlas (30, 31) demonstrated that the neural constructs were most correlated to early developmental time points and least correlated to later adult time points (Dataset S1). For example, Spearman's coefficients for day 16 and day 21 neural constructs were higher for all comparisons to eight postconception week (PCW) samples ($[\rho] \geq 0.82$, all brain regions) than 30-y-old adult samples ($[\rho] \leq 0.76$, all brain regions) (30, 31). However, given the timing of our differentiation protocol, the neural constructs likely represent developmental time points before the earliest available RNA-Seq data (8 PCW) from the Allen Brain Atlas (30, 31).

RNA-Seq data were then analyzed by EBSeq (32) to identify genes up-regulated within the neural constructs compared with undifferentiated human ES cells (Dataset S2). Characteristic gene ontology (GO) clusters were identified from the resulting gene sets using the DAVID Bioinformatics Database Functional Annotation Tool (Dataset S2) (33, 34). Genes threefold up-regulated with an EBSeq false discovery rate (FDR) ≤ 0.005 for day 21 neural constructs relative to H1 ES cells were enriched within GO categories that included neurogenesis (GO:0022008, 206 genes), forebrain development (GO:0030900, 40 genes), hindbrain development (GO:0030902, 26 genes), synaptic transmission (GO:0007268, 112 genes), and vasculature development (GO:0001944, 61 genes) (Dataset S2). RNA-Seq also identified expressed genes for phenotypes important to neurogenesis (Datasets S2 and S3), such as GABAergic neurons (e.g., GABA receptors), glutamatergic neurons (e.g., VGLUT2 and VGAT), cortical neurons (reelin/RELN, BRN2/POU3F2, CTIP2/BCL11B, etc.), synaptic markers (e.g., synapsins and synaptic vesicle components), and glial cells (GFAP, PDGFRA, GLAST/SLC1A3, etc.) (9, 35–39).

Immunofluorescence imaging was used to investigate cellular organization within the neural constructs. Neural progenitor cells differentiated and self-assembled into layered βIII-tubulin$^+$ and GFAP$^+$ cells that extended around the circumference of the neural constructs by day 9 of culture on PEG hydrogels (*SI Appendix*, Fig. S2). By day 21, sample thickness varied from ~50 μm in the center to >350 μm in outer regions of the neural constructs (Fig. 1), where complex cellular organization was most pronounced. Ki67$^+$ proliferative layers (*SI Appendix*, Fig. S3) and radially organized cells that expressed GFAP, phospho-vimentin (p-VIM), and/or SOX2 were each identified within the neural constructs (*SI Appendix*, Fig. S4) (9, 38, 39). Immunofluorescence imaging revealed markers for GABAergic neurons (GABA; Fig. 2*A*) and glutamatergic neurons (VGLUT2; Fig.

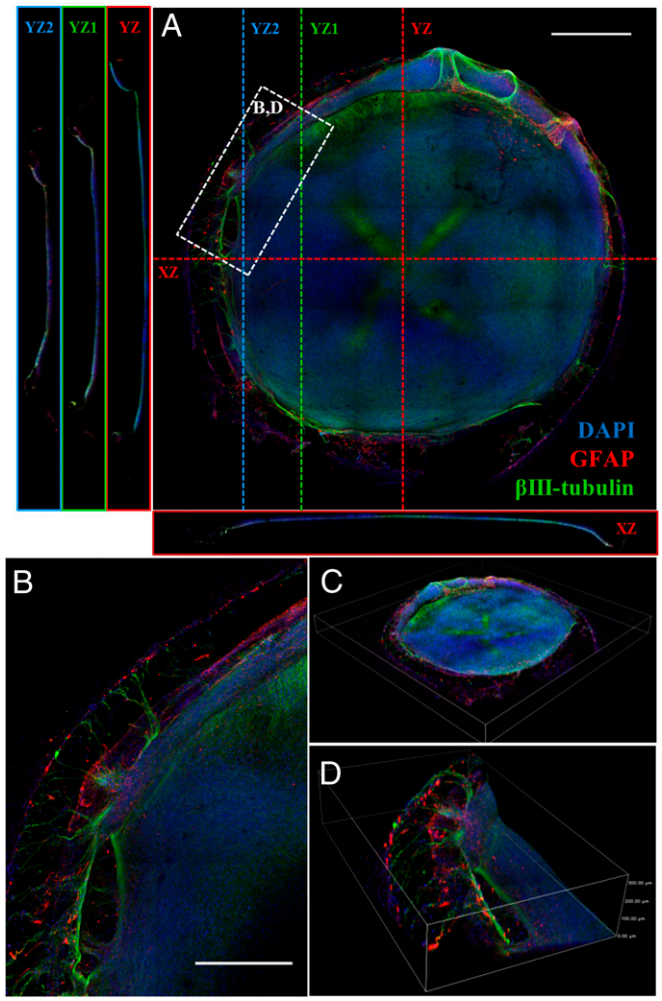

Fig. 1. Morphological characteristics of neural constructs. Human embryonic stem cell-derived precursor cells were cocultured on polyethylene glycol (PEG) hydrogels in 24-well Transwell inserts. Neural progenitor cells (NPCs) were seeded on synthetic PEG hydrogels (day 0), followed by endothelial cells (ECs) and mesenchymal stem cells (MSCs) at day 9 and microglia/macrophage precursors (MGs) at day 13 (*SI Appendix*, Fig. S1). (*A* and *B*) Maximum projection *Z* stack (525-μm thickness) and slice views (NIS Elements) illustrating βIII-tubulin (green), GFAP (red), and DAPI (blue) for a day 21 neural construct. XZ and YZ cross-sections are illustrated in the regions indicated by dashed lines. The boxed region in *A* is illustrated in *B*. (*C* and *D*) Volume view images (NIS Elements) corresponding to (*C*) the full neural construct shown in *A* (6,300 μm × 6,300 μm × 550 μm) and (*D*) the region shown in *B* (1,570 μm × 2,290 μm × 300 μm). (Scale bar in *A*, 1,000 μm and *B*, 500 μm.)

2*B*), and reelin$^+$ (RELN, Fig. 2*C*), calretinin$^+$ (CALB2, Fig. 2*C*), Brn2$^+$ (POU3F2, Fig. 2*D*), Ctip2$^+$ (BCL11B, Fig. 2*E*), and Tbr1$^+$ layers were also evident (Fig. 2*E*) (9, 35–37). Thus, neural phenotypes identified by immunofluorescence imaging were in agreement with the RNA-Seq results (Datasets S2 and S3).

Human ES cell-derived endothelial cells and mesenchymal stem cells were added to the neural constructs after neural progenitor cells had self-assembled into multilayers with radially organized neural and glial populations (*SI Appendix*, Fig. S2) (9, 37, 38) to mimic the recruitment of blood vessels by the neuroepithelium (15). The neural constructs were characterized by extensive capillary networks by day 21 (Fig. 3*A*; *SI Appendix*, Fig. S5), which associated with radially oriented glial cells (Fig. 3 *B–D*) and penetrated into neuronal layers (*SI Appendix*, Fig. S5) (13–15). RNA-Seq demonstrated that the neural constructs expressed many vascular genes [day 21: 122 genes, GO:0001944 vasculature development, transcripts per million (TPM) > 16; Dataset S4], including blood-vessel–promoting growth factors (e.g., VEGFA) that were also detected in control samples lacking vascular cells (Dataset S3). Because factors such as VEGF were not added exogenously, cellular signaling within the neural constructs provided the necessary cues for the formation of interconnected vascular networks, which is consistent with the recruitment of capillaries by cells within the neuroepithelium (15).

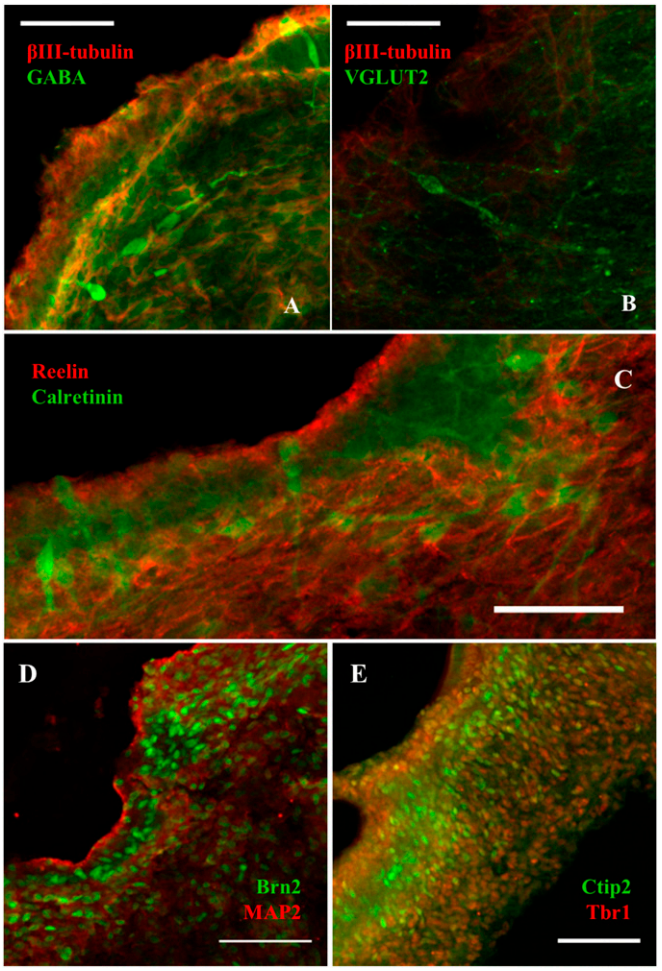

Fig. 2. Neural differentiation within the neural constructs. Cryosectioned samples illustrating neuronal phenotypes after 21 d of growth on PEG hydrogels: (*A*) βIII-tubulin (red) and GABA (green), (*B*) βIII-tubulin (red) and VGLUT2 (green), (*C*) reelin (red) and calretinin (green), (*D*) MAP2 (red) and Brn2 (green), and (*E*) Ctip2 (green) and Tbr1 (red). (Scale bars in *A–C*, 50 μm and *D* and *E*, 100 μm.)

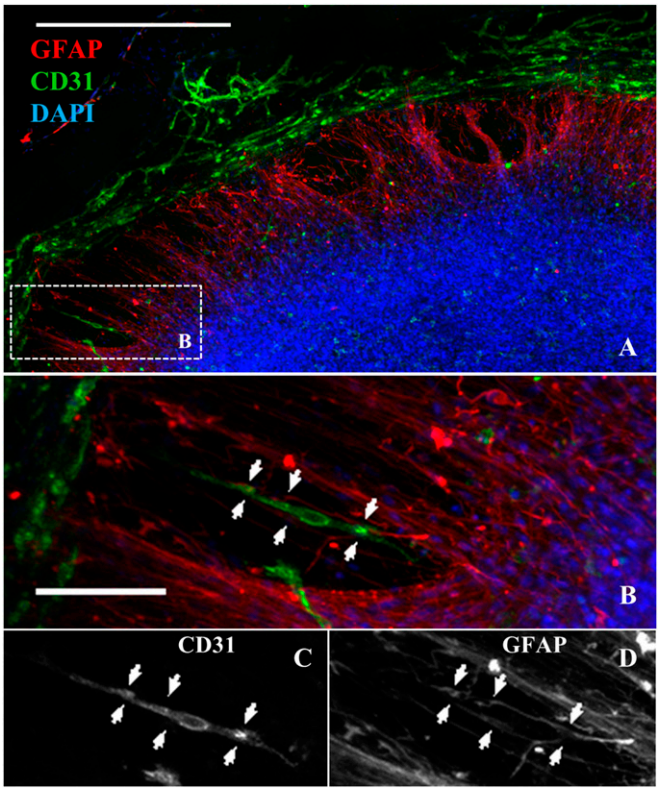

Fig. 3. Vascular network formation within the neural constructs. (*A* and *B*) Immunofluorescence for endothelial cells (CD31, green), glial cells (GFAP, red), and nuclei (DAPI, blue) for a day 21 neural construct. (*B*) Zoom of the boxed region shown in *A* to illustrate association and alignment for a capillary tubule and radially oriented glial cells (arrows). The cells in *B* are shown as single channel grayscale images for (*C*) CD31 and (*D*) GFAP. [Scale bars in *A*, 250 μm and *B–D*, 100 μm (shown in *B*).]

Microglia/macrophage precursors were derived by differentiating H1 ES cells through mesendoderm and hemogenic endothelium lineages (40), which resemble early precursors in the yolk sac that contribute to microglia in vivo (41). The microglia/macrophage precursors were CD11b$^+$CD14$^+$ by FACS analysis (*SI Appendix*, Fig. S1) and phagocytosed yeast particles (Movie S1). Iba1$^+$ microglia begin to populate the human brain as early as 4.5 gestational weeks (GW), but minimally interact with early blood vessels (11). Therefore, the microglia/macrophage precursors were added to the neural constructs after initial vascular network assembly (11). Characteristic microglia genes were up-regulated relative to control samples (Fig. 4*A*) and were expressed at days 16 and 21 (*SI Appendix*, Fig. S6 and Dataset S3) when microglia/macrophage precursors were incorporated into the neural constructs (10–12). TREM2, IBA1/AIF1, and other microglial genes were detectable by RNA-Seq only when microglia/macrophage precursors were incorporated into the neural constructs (Fig. 4*A*). By day 21, Iba1$^+$ cells were dispersed throughout the neural constructs (*SI Appendix*, Fig. S6), associated with endothelial tubules (Fig. 4*B* and *SI Appendix*, Fig. S6), and adopted both amoeboid and ramified morphologies (Fig. 4*B* and *SI Appendix*, Fig. S6) (10–12).

RNA-Seq and linear support vector machines were then used to build a predictive model for neurotoxicity based on changes in global gene expression by neural constructs exposed to known toxins and nontoxic controls (Fig. 5 and *SI Appendix*, Fig. S7 and Datasets S5 and S6) (42–46). Neurotoxicity was evaluated using a set of 31 control compounds and 39 toxins with previous literature support for toxicity (Dataset S5). Control chemicals included common food additives or pharmaceuticals with no known neurotoxicity.

Dosage was based on previous in vitro or in vivo data for toxic and nontoxic compounds, which included blood serum concentrations (such as for pharmaceuticals) or previously published screening conditions when available or set at 10 μM when data were not available. Replicate day 14 neural constructs were continuously exposed to test compounds through day 16 (2 d of exposure) or day 21 (7 d of exposure), and then harvested for RNA-Seq (Datasets S7 and S8) and machine learning analysis (Dataset S6).

We used two standard hold-out testing methods for evaluation to avoid overly optimistic prediction of accuracy (45–47): (*i*) A nearly unbiased (slightly pessimistic) leave-one-out cross-validation and (*ii*) an unbiased blinded trial with a single hold-out set. For leave-one-out cross-validation, there were 60 compounds in the training set and the method proceeded in 60 steps. In each step a different data point was held out of the training set, the support vector machine was trained on the remaining data points, and a prediction was made for the held-aside data point. Hence every data point was a test case exactly once, for a model trained without that data point. Results were aggregated over all of the folds, or test cases, to estimate how well the support vector machine trained on all data will perform on a new data point

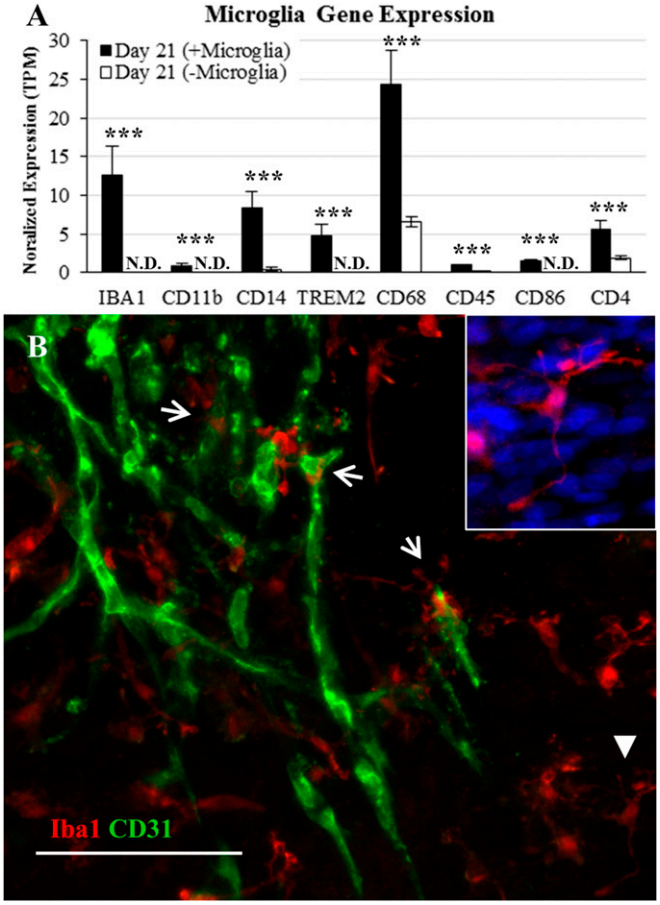

Fig. 4. Incorporation of microglia into neural constructs. (*A*) Gene expression for neural constructs with or without microglia (Dataset S3, Quality Control Experiments; N.D., not detected). Statistical analysis was conducted using a Student's *t* test (TPM ± SD; ***$P < 0.001$; $n = 4$ replicate samples each). (*B*) Iba1 (microglia, red) and CD31 (endothelial cells, green) expression for a day 21 neural construct. Microglia adopt ramified morphologies (e.g., closed arrow) and associate with capillary tubules (e.g., open arrows). (*Inset*) Iba1 (red) and DAPI (blue) expression for the cell pointed out by the closed arrow (*Bottom, Right* corner) and surrounding nuclei. Image is brightened for clarity. (Scale bar, 100 μm.)

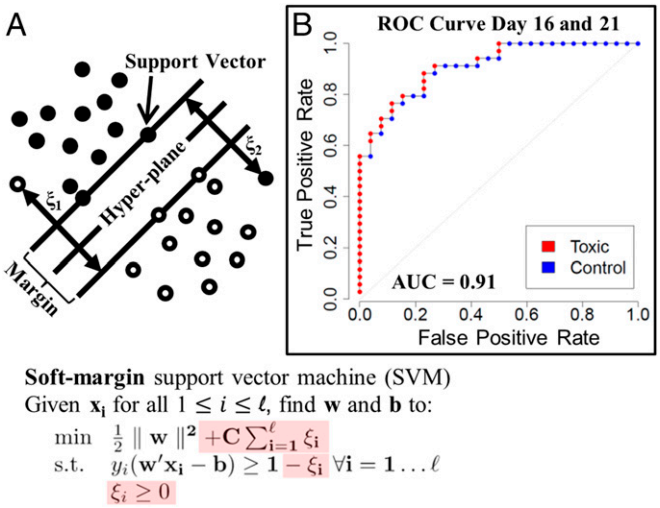

Soft-margin support vector machine (SVM)
Given $\mathbf{x_i}$ for all $1 \le i \le \ell$, find $\mathbf{w}$ and $\mathbf{b}$ to:

$$\min \ \tfrac{1}{2} \| \mathbf{w} \|^2 + C \sum_{i=1}^{\ell} \xi_i$$
$$\text{s.t.} \ \ y_i(\mathbf{w}'\mathbf{x_i} - \mathbf{b}) \ge 1 - \xi_i \ \forall \mathbf{i} = 1 \ldots \ell$$
$$\xi_i \ge 0$$

Fig. 5. Machine learning predictions. (*A*) A linear support vector machine (SVM) for a 2D problem, where an ($n - 1$)-dimensional hyperplane reduces to a line that separates the classes (filled vs. open circles) and maximizes the closest points between classes (the support vectors, which fix the position and orientation of the hyperplane). The $\mathbf{x_i}$s are the examples (points in *A*), the $\mathbf{y_i}$s are their labels (filled or open in *A*), and $\mathbf{w}$ is the weight vector, or vector of coefficients on the features (the dimensions). The linear SVM's output is the weight vector $\mathbf{w}$ and the other coefficient $\mathbf{b}$. To make a prediction, the SVM computes the number $\mathbf{w}'\mathbf{x_i} - \mathbf{b}$, and outputs the label 0 (nontoxic, for our application) if this number is less than 0, and 1 otherwise. The extensions required for the soft margin version of the SVM are highlighted in pink in the equation, which minimizes the sum of the distances between incorrectly classified training points (ξ_i) in addition to the margin, and is used when the data are not linearly separable (43). (*B*) The ROC curves are shown for the data averaged from days 16 (2-day dosing) and 21 (7-day dosing) (Dataset S6). The ROC curve plots true positive rate on the *y* axis against the false positive rate (1 – specificity) on the *x* axis as the threshold is varied (*SI Appendix, SI Materials and Methods* shows additional details).

(compound). Performance estimates are shown in the form of receiver operating characteristic (ROC) curves (Fig. 5 and *SI Appendix*, Fig. S7). For the second method, the unbiased blinded trial used the predictive model generated from the training set to make predictions on a separate hold-out set, including estimates of accuracy and area under the ROC curve (AUC). The leave-one-out cross-validation method has lower variance than a single train/test split because it tests on all of the compounds of the training set, but it is a slightly pessimistic estimate of future performance because each training set is slightly smaller (one less) than the actual training set.

Leave-one-out cross-validation was used to evaluate neural constructs exposed to a training set of 34 toxins and 26 nontoxic controls (Datasets S5 and S6). The area under the ROC curves for the training compounds were 0.86 on day 16 (*SI Appendix*, Fig. S7), 0.88 on day 21 (*SI Appendix*, Fig. S7), and 0.91 for data averaged from both days (Fig. 5*B*). Thus, the support vector machine produced an estimate of future data ≥0.86 for each day individually and 0.91 using data from two developmental time points. Additionally, a wrapper-based approach of recursive feature elimination (48) demonstrated that the number of genes could be reduced to 1,000 without harming accuracy (Dataset S6). Unbiased hold-out testing was then used to predict toxicity for a set of 10 blinded compounds that were not in the initial training set (five toxins, five nontoxic controls, Dataset S5) and were unknown to researchers generating the support vector machine model until after the predictions were made. The support vector machine model was generated using the full set of ~19,000 genes and data were averaged from days 16 and 21 training sets to make predictions, which produced probabilities for ranking the blinded compounds from most likely toxic to least

likely toxic (Dataset S6). In addition, we used a threshold of 0.5 to make definitive predictions, labeling every chemical with probability ≤0.5 as nontoxic and all others toxic. The area under the ROC curve generated for the ranking of the blinded set was 0.92, which is in agreement with the training experiment. Importantly, all compounds except oleic acid (a false positive) were properly assigned as toxic or nontoxic (Dataset S6). Therefore, the predictive model correctly classified 9 of 10 compounds in the blinded trial.

Discussion

The complexity of the developing human brain complicates efforts to assess developmental neurotoxicity in vitro, as the underlying mechanisms may include selective cell death, delayed or aberrant differentiation, suppressed neurotransmission, disruption of the blood–brain barrier, or modulation of inflammatory signals by glial or microglial cells (16–20). Thus, an in vitro model to predict human neurotoxicity needs to recapitulate a diversity of cellular interactions during human brain development and should be reproducible both within an experiment and between experiments performed on different days or at different sites. Human ES and iPS cells offer a consistent, scalable source for diverse neural cell types (49), including neural precursors that differentiate and self-assemble through mechanisms that recapitulate aspects of brain development (50–52).

Whereas previous studies have provided impressive demonstrations of the capacity for neuronal precursor cells to self-assemble into 3D "organoids" (52), current models lack vascular and microglial components and use procedures that are not easily scalable for enhanced-throughput or standardized screening approaches. The neural constructs described here incorporated vascular and microglial components and were produced with high sample uniformity by culturing precursors derived from the H1 human ES cell line on chemically defined hydrogels under serum-free conditions. Matrigel is widely used as a scaffold for organoid culture (53), but varies between batches and is a poorly defined mixture of proteins, including many potent growth factors and extracellular matrix components (54). In contrast, self-assembly of precursors into neural constructs here occurred on minimally complex PEG hydrogels (27, 28), with the only bioactive components being matrix metalloproteinase (MMP)-degradable peptide cross-links permissive to proteolytic remodeling (55) and pendant Cys-Arg-Gly-Asp-Ser (CRGDS) peptide to promote cell adhesion (56). By producing uniform samples with diverse features that include neuronal, glial, vascular, and microglial populations, the 3D neural constructs should be suitable for predicting toxicities for chemicals that target a wide range of interactions important to brain development.

The diversity of potential mechanisms that might be disrupted during neurodevelopment presents particular challenges when choosing the readout for identifying a chemical compound as toxic (5). Previously, transcriptomics approaches have been applied to evaluate developmental neurotoxicity in vitro (57, 58), including a "murine neural embryonic stem cell test" that was used to identify predictive genes for 10 test compounds (58). Here, RNA-Seq and machine learning were chosen to leverage the biological complexity of the neural constructs by simultaneously assessing changes in global gene expression for all cellular interactions that might be targeted by neurotoxic chemicals. The high dynamic range for RNA-Seq provides sensitive detection of gene expression changes for cells within the neural constructs, even for minor cell subpopulations, whereas linear support vector machines have previously been shown to perform well using gene expression data (45, 46). The machine learning model correctly identified 9 of 10 blinded chemicals as toxic or nontoxic (with one false positive), which compares favorably with the expected accuracy when using animal testing to predict human neurotoxicity (7).

It has been demonstrated that accurate machine learning algorithms can be constructed with significantly fewer examples (data points or training compounds) than features (variables or genes) (44–46), but 60 training compounds is still an exceptionally small dataset given that ∼19,000 genes were assessed. Therefore, it is a reasonable expectation that predictive accuracy can be improved further by adding more toxins and controls to the training set. For example, our day 16 model correctly predicts the training compound cadmium to be toxic, but our day 21 model does not (Dataset S6). Nevertheless, there are alternative linear separators for day 21 data (with nearly as large margins) that would correctly classify cadmium. Such an alternative linear separator is constructed for the full training set that includes cadmium, such as that used to make predictions for the blinded compounds; this observation supports the assumption that the model would be improved with additional training data. By expanding the training set to include additional compounds with characteristics similar to cadmium, the learning algorithm would construct such an alternative linear separator even if cadmium were held out. Similar improvements might be expected by including other compounds to account for distinct toxic effects that are either underrepresented or not represented at all with the current training set, and incorporation of such information to improve the predictive model is a particular advantage of our approach.

Machine learning algorithms are also dependent on training compounds that can be definitively assigned. Therefore, initial misclassification of a compound would result in an incorrect prediction even if the machine learning algorithm makes an accurate assessment, such as if a control compound was dosed at a toxic concentration. For example, oleic acid was chosen as a nontoxic control for the blinded set and was dosed at a lower concentration than values reported for human serum (59), but was predicted to be toxic by the machine learning algorithm. It was previously reported that free oleic acid content transiently increases in the brains of postnatal day 1 rats, which was correlated to a neurotrophic role during axonogenesis (60). Thus, a potential toxic outcome for oleic acid might arise if the neurotrophic effect is tightly regulated, because elevated expression could disrupt normal developmental timing. This example highlights the uncertainty that limits current efforts to predict developmental neurotoxicity, as mechanisms that might disrupt human brain development are largely unknown, and susceptibility to a particular chemical may be dependent on the developmental timeframe being modeled.

The protocol described here produces neural tissue constructs with consistent gene expression profiles that are useful for predicting neurotoxicity, but the extent to which they mimic normal human neural development and function remains largely unexplored. For example, whereas the neural constructs expressed genes that were enriched for GO terms associated with mechanisms of neurotransmission (e.g., synaptic transmission), functional studies such as electrophysiology were not performed. Although we were successful in promoting the self-assembly of vascular networks within the neural constructs, the current model does not yet include a functional, perfused blood–brain barrier. The blood–brain barrier prevents many toxic compounds from entering the brain, which presents challenges when choosing the dose for chemicals in the training set using the current model. For example, animal studies suggest that oleic acid does not cross the blood–brain barrier at normal serum concentrations (61), and direct application to the neural tissue could therefore explain our false positive result. Several groups have now reported flow-based platforms for perfusing vascular networks (62, 63). Pairing such actively perfused devices with the vascularized 3D neural constructs described here may promote more advanced differentiation and growth, whereas the incorporation of blood–brain barrier function would be beneficial for investigating the delivery of therapeutic agents and could improve the predictive accuracy of our model by delivering toxic chemicals in a more physiologically relevant manner.

Materials and Methods

Detailed protocols for deriving precursor cells, assembly on synthetic hydrogels, immunofluorescence imaging, toxicity screening, RNA processing, RNA-Seq methods, gene expression analysis, and machine learning are provided in *SI Appendix, SI Materials and Methods*.

ACKNOWLEDGMENTS. The authors thank Mackenzie Holland, Collin Edington, and Angela Xie for editing the manuscript. The National Institutes of Health (NIH) in collaboration with the Defense Advanced Research Projects Agency and the US Food and Drug Administration created the Microphysiological Systems (MPS) program to develop improved in vitro human cellular models to more accurately predict whether drugs will be safe and effective. The MPS program is supported by NIH 1UH2TR000506-01, 3UH2TR000506-02S1, and 4UH3TR000506-03. Additional funding was provided by NIH R21EB016381-01. M.P.S. acknowledges a donation in the memory of Gerald E. Whitbeck (generously provided by his family and the Follett Corp.).

1. Fabre KM, Livingston C, Tagle DA (2014) Organs-on-chips (microphysiological systems): Tools to expedite efficacy and toxicity testing in human tissue. *Exp Biol Med (Maywood)* 239(9):1073–1077.
2. Judson R, et al. (2014) In vitro and modelling approaches to risk assessment from the U.S. Environmental Protection Agency ToxCast programme. *Basic Clin Pharmacol Toxicol* 115(1):69–76.
3. Crofton KM, et al. (2011) Developmental neurotoxicity testing: Recommendations for developing alternative methods for the screening and prioritization of chemicals. *ALTEX* 28(1):9–15.
4. Grandjean P, Landrigan PJ (2014) Neurobehavioural effects of developmental toxicity. *Lancet Neurol* 13(3):330–338.
5. Bal-Price A, et al. (2015) International STakeholder NETwork (ISTNET): Creating a developmental neurotoxicity (DNT) testing road map for regulatory purposes. *Arch Toxicol* 89(2):269–287.
6. Hay M, Thomas DW, Craighead JL, Economides C, Rosenthal J (2014) Clinical development success rates for investigational drugs. *Nat Biotechnol* 32(1):40–51.
7. Olson H, et al. (2000) Concordance of the toxicity of pharmaceuticals in humans and in animals. *Regul Toxicol Pharmacol* 32(1):56–67.
8. Rice D, Barone S, Jr (2000) Critical periods of vulnerability for the developing nervous system: Evidence from humans and animal models. *Environ Health Perspect* 108(Suppl 3):511–533.
9. Bystron I, Blakemore C, Rakic P (2008) Development of the human cerebral cortex: Boulder Committee revisited. *Nat Rev Neurosci* 9(2):110–122.
10. Kettenmann H, Hanisch UK, Noda M, Verkhratsky A (2011) Physiology of microglia. *Physiol Rev* 91(2):461–553.
11. Verney C, Monier A, Fallet-Bianco C, Gressens P (2010) Early microglial colonization of the human forebrain and possible involvement in periventricular white-matter injury of preterm infants. *J Anat* 217(4):436–448.
12. Arnold T, Betsholtz C (2013) The importance of microglia in the development of the vasculature in the central nervous system. *Vasc Cell* 5(1):4.
13. Stolp H, Neuhaus A, Sundramoorthi R, Molnár Z (2012) The long and the short of it: Gene and environment interactions during early cortical development and consequences for long-term neurological disease. *Front Psychiatry* 3:50.
14. Marín-Padilla M (2012) The human brain intracerebral microvascular system: Development and structure. *Front Neuroanat* 6:38.
15. James JM, Mukouyama YS (2011) Neuronal action on the developing blood vessel pattern. *Semin Cell Dev Biol* 22(9):1019–1027.
16. Lidsky TI, Schneider JS (2003) Lead neurotoxicity in children: Basic mechanisms and clinical correlates. *Brain* 126(Pt 1):5–19.
17. Block ML, Hong JS (2005) Microglia and inflammation-mediated neurodegeneration: Multiple triggers with a common mechanism. *Prog Neurobiol* 76(2):77–98.
18. de Groot MW, Westerink RHS, Dingemans MML (2013) Don't judge a neuron only by its cover: Neuronal function in in vitro developmental neurotoxicity testing. *Toxicol Sci* 132(1):1–7.
19. Monnet-Tschudi F, Zurich MG, Honegger P (2007) Neurotoxicant-induced inflammatory response in three-dimensional brain cell cultures. *Hum Exp Toxicol* 26(4):339–346.
20. Eskes C, Juillerat-Jeanneret L, Leuba G, Honegger P, Monnet-Tschudi F (2003) Involvement of microglia-neuron interactions in the tumor necrosis factor-alpha release, microglial activation, and neurodegeneration induced by trimethyltin. *J Neurosci Res* 71(4):583–590.
21. Thomson JA, et al. (1998) Embryonic stem cell lines derived from human blastocysts. *Science* 282(5391):1145–1147.
22. Yu J, et al. (2007) Induced pluripotent stem cell lines derived from human somatic cells. *Science* 318(5858):1917–1920.
23. Takahashi K, et al. (2007) Induction of pluripotent stem cells from adult human fibroblasts by defined factors. *Cell* 131(5):861–872.
24. Chambers SM, et al. (2009) Highly efficient neural conversion of human ES and iPS cells by dual inhibition of SMAD signaling. *Nat Biotechnol* 27(3):275–280.
25. Vodyanik MA, et al. (2010) A mesoderm-derived precursor for mesenchymal stem and endothelial cells. *Cell Stem Cell* 7(6):718–729.
26. Stratman AN, Davis GE (2012) Endothelial cell-pericyte interactions stimulate basement membrane matrix assembly: Influence on vascular tube remodeling, maturation, and stabilization. *Microsc Microanal* 18(1):68–80.
27. Fairbanks BD, et al. (2009) A versatile synthetic extracellular matrix mimic via thiol-norbornene photopolymerization. *Adv Mater* 21(48):5005–5010.
28. Hansen TD, et al. (2014) Biomaterial arrays with defined adhesion ligand densities and matrix stiffness identify distinct phenotypes for tumorigenic and nontumorigenic human mesenchymal cell types. *Biomater Sci* 2(5):745–756.
29. Hou Z, et al. (2015) A cost-effective RNA sequencing protocol for large-scale gene expression studies. *Sci Rep* 5:9570.
30. Miller JA, et al. (2014) Transcriptional landscape of the prenatal human brain. *Nature* 508(7495):199–206.
31. Hawrylycz MJ, et al. (2012) An anatomically comprehensive atlas of the adult human brain transcriptome. *Nature* 489(7416):391–399.
32. Leng N, et al. (2013) EBSeq: An empirical Bayes hierarchical model for inference in RNA-seq experiments. *Bioinformatics* 29(8):1035–1043.
33. Huang W, Sherman BT, Lempicki RA (2009) Systematic and integrative analysis of large gene lists using DAVID bioinformatics resources. *Nat Protoc* 4(1):44–57.
34. Ashburner M, et al.; The Gene Ontology Consortium (2000) Gene ontology: Tool for the unification of biology. *Nat Genet* 25(1):25–29.
35. Zecevic N, Milosevic A, Rakic S, Marín-Padilla M (1999) Early development and composition of the human primordial plexiform layer: An immunohistochemical study. *J Comp Neurol* 412(2):241–254.
36. Ip BK, Bayatti N, Howard NJ, Lindsay S, Clowry GJ (2011) The corticofugal neuron-associated genes ROBO1, SRGAP1, and CTIP2 exhibit an anterior to posterior gradient of expression in early fetal human neocortex development. *Cereb Cortex* 21(6):1395–1407.
37. Bystron I, Rakic P, Molnár Z, Blakemore C (2006) The first neurons of the human cerebral cortex. *Nat Neurosci* 9(7):880–886.
38. Zecevic N (2004) Specific characteristic of radial glia in the human fetal telencephalon. *Glia* 48(1):27–35.
39. Lui JH, Hansen DV, Kriegstein AR (2011) Development and evolution of the human neocortex. *Cell* 146(1):18–36.
40. Uenishi G, et al. (2014) Tenascin C promotes hematoendothelial development and T lymphoid commitment from human pluripotent stem cells in chemically defined conditions. *Stem Cell Rep* 3(6):1073–1084.
41. Ginhoux F, et al. (2010) Fate mapping analysis reveals that adult microglia derive from primitive macrophages. *Science* 330(6005):841–845.
42. Vapnik VN (1998) *Statistical Learning Theory* (Wiley, New York).
43. Cortes C, Vapnik V (1995) Support-Vector Networks. *Mach Learn* 20(3):273–297.
44. Furey TS, et al. (2000) Support vector machine classification and validation of cancer tissue samples using microarray expression data. *Bioinformatics* 16(10):906–914.
45. Struyf J, Dobrin S, Page D (2008) Combining gene expression, demographic and clinical data in modeling disease: A case study of bipolar disorder and schizophrenia. *BMC Genomics* 9:531.
46. Hardin J, et al. (2004) Evaluation of multiple models to distinguish closely related forms of disease using DNA microarray data: An application to multiple myeloma. *Stat Appl Genet Mol Biol* 3:e10.
47. Golub TR, et al. (1999) Molecular classification of cancer: Class discovery and class prediction by gene expression monitoring. *Science* 286(5439):531–537.
48. Guyon I, Weston J, Barnhill S, Vapnik V (2002) Gene selection for cancer classification using support vector machines. *Mach Learn* 46(1-3):389–422.
49. Zhang SC, Wernig M, Duncan ID, Brüstle O, Thomson JA (2001) In vitro differentiation of transplantable neural precursors from human embryonic stem cells. *Nat Biotechnol* 19(12):1129–1133.
50. Stein JL, et al. (2014) A quantitative framework to evaluate modeling of cortical development by neural stem cells. *Neuron* 83(1):69–86.
51. Gaspard N, Vanderhaeghen P (2010) Mechanisms of neural specification from embryonic stem cells. *Curr Opin Neurobiol* 20(1):37–43.
52. Eiraku M, Sasai Y (2012) Self-formation of layered neural structures in three-dimensional culture of ES cells. *Curr Opin Neurobiol* 22(5):768–777.
53. Lancaster MA, Knoblich JA (2014) Organogenesis in a dish: Modeling development and disease using organoid technologies. *Science* 345(6194):1247125.
54. Hughes CS, Postovit LM, Lajoie GA (2010) Matrigel: A complex protein mixture required for optimal growth of cell culture. *Proteomics* 10(9):1886–1890.
55. Nagase H, Fields GB (1996) Human matrix metalloproteinase specificity studies using collagen sequence-based synthetic peptides. *Biopolymers* 40(4):399–416.
56. Pierschbacher MD, Ruoslahti E (1984) Cell attachment activity of fibronectin can be duplicated by small synthetic fragments of the molecule. *Nature* 309(5963):30–33.
57. Krug AK, et al. (2013) Human embryonic stem cell-derived test systems for developmental neurotoxicity: A transcriptomics approach. *Arch Toxicol* 87(1):123–143.
58. Pennings JLA, Theunissen PT, Piersma AH (2012) An optimized gene set for transcriptomics based neurodevelopmental toxicity prediction in the neural embryonic stem cell test. *Toxicology* 300(3):158–167.
59. Teubert A, Thome J, Büttner A, Richter J, Irmisch G (2013) Elevated oleic acid serum concentrations in patients suffering from alcohol dependence. *J Mol Psychiatry* 1(1):13.
60. Polo-Hernández E, De Castro F, García-García AG, Tabernero A, Medina JM (2010) Oleic acid synthesized in the periventricular zone promotes axonogenesis in the striatum during brain development. *J Neurochem* 114(6):1756–1766.
61. Edmond J (2001) Essential polyunsaturated fatty acids and the barrier to the brain: The components of a model for transport. *J Mol Neurosci* 16(2-3):181–193, discussion 215–221.
62. Moya ML, Hsu Y, Lee AP, Hughes CCW, George SC (2013) In vitro perfused human capillary networks. *Tiss. Eng. Part C Methods* 19(9):730–737.
63. Domansky K, et al. (2010) Perfused multiwell plate for 3D liver tissue engineering. *Lab Chip* 10(1):51–58.